



Active integrated fabrication method and evaluation of polymer with microneedles LED light source integration

Xiaoning Zhang¹ · Qingxin Han³ · Xiaoqing Hu² · Lei Zhang³ · Xiaoya Kang¹ · Ming Li¹ · Qiang Gao¹ · Fengyi Liu¹ · Jingyao Sun¹ · Jingxian Zhu² · Jian Zhuang^{1,4}

Received: 20 May 2024 / Accepted: 19 July 2024

© The Author(s), under exclusive licence to Springer-Verlag GmbH Germany, part of Springer Nature 2024

Abstract

This article proposes a new process for fabricating a polymer microneedles (MNs) patch integrated with an LED light source (LED-HEMA/MN, LH-MN) using ultraviolet (UV) curing technology. Hydroxyethyl methacrylate (HEMA) is used as the base material, with a focus on studying the active integrated fabrication process of the MNs patch. The study also investigates the morphology, size, mechanical properties, ex vivo skin penetration performance, operating temperature, and performance optimization of the LH-MN. The experimental results show that the LH-MN fabricated using the optimal process has a good appearance, high molding rate, short production cycle, and excellent mechanical properties. It can effectively penetrate the skin without the risk of thermal injury. In addition, the MNs patch (LED-HEMA/HEA-MN, LHH-MN) prepared by optimizing and modifying with hydroxyethyl acrylate (HEA) possesses good flexibility and mechanical properties. It can adapt to different shapes and locations of the affected area, greatly enhancing the practicality of the MNs.

1 Introduction

Light treatment (LT), also known as photochemotherapy, has effects such as promoting tissue repair, promoting blood circulation, and relieving pain (Dompe et al. 2020; Glass 2020, 2021). In recent years, LT has been widely used in the treatment of various diseases, such as wound healing (Dehghanpour et al. 2023), oral mucositis (Courtois et al. 2021) and hair loss (Roets 2023). However, biological tissues, due to their high scattering and low absorption

optical properties, make it difficult for light to penetrate deep tissues, resulting in LT being mainly used for the treatment of superficial diseases (Cheong et al. 1990).

MNs are a new type of drug delivery method in modern drug delivery technology. It is a patch made up of an array of tiny needles. MNs can accurately penetrate the stratum corneum without touching pain nerves, which can avoid skin damage and pain, while achieving targeted transdermal drug delivery, thereby improving treatment effects (Xue et al. 2024; Lim and Kim 2022; Yin et al. 2023). Common preparation materials mainly include silicon, metal, and polymer materials, among which polymer materials have the advantages of abundant sources, low cost, good biocompatibility, and good biodegradability, and have great potential in the preparation of MNs (Luo et al. 2023; Zhang et al. 2021, 2022). With the development and upgrading of polymer MNs, they are no longer limited to the transdermal delivery of drugs alone, and the transdermal delivery of light is attracting more and more attention.

The development and advancement of polymer microneedles have transcended their original limitation to mere transdermal drug delivery. The combination of light and drug therapy, as well as the precise delivery of light, is garnering increasing attention. For instance, Researchers used red light at 650–675 nm in conjunction with

Jingxian Zhu and Jian Zhuang have contributed equally.

✉ Jian Zhuang
zhuangjian@mail.buct.edu.cn

¹ School of Mechanical and Electrical Engineering, Beijing University of Chemical Technology, Beijing 100029, China

² Department of Sports Medicine, Peking University Third Hospital, Institute of Sports Medicine of Peking University, Beijing 100191, China

³ Department of Arthroscopy and Sports Medicine, Wangjing Hospital, China Academy of Chinese Medical Sciences, Beijing 100102, China

⁴ Institute of Plastics Machinery and Plastic Engineering, Beijing University of Chemical Technology, No. 15 North Sanhuan East Road, Chaoyang District, Beijing 100029, China

microneedles for the treatment of androgenetic alopecia, which effectively improved the patients' hair loss conditions, promoted hair growth, and had a high safety profile (Zheng et al. 2024). Researchers developed a multifunctional cryo-microneedle patch for trackable photodynamic therapy, requiring external irradiation of green light at 532 nm during the treatment process. This microneedle patch has shown significant efficacy in eliminating tumors, highlighting its broad clinical prospects (Li et al. 2024). Furthermore, Researchers used microneedles for localized light delivery to melanoma cells, with a highly fixed device that can be mounted in a cell culture dish and connected to an external power source with blue light at 467 nm, providing a new strategy for the treatment of melanoma (Wu et al. 2022).

However, current research still relies on external light sources, and during the treatment process, it is required to keep the light source stable and immovable, which limits the patient's activity space and range. In addition, when treating deep skin tissues, due to the barrier effect of the skin, the external light source is difficult to provide sufficient light intensity. LED light sources, with their compact size and component volume, offer great convenience for integration into various devices, making lighting design more flexible and diverse. The wireless power supply technology achieved through electromagnetic coils allows LED light sources to be independent of external power sources (Li et al. 2020a). Currently, researchers have successfully implanted such wirelessly powered LED light sources under the skin of mice for the treatment of subcutaneously transplanted tumors, achieving significant therapeutic effects (Yamagishi et al. 2018). Furthermore, other researchers have implanted wirelessly powered LED light sources in mice, triggering the release of nitric oxide (NO), which has shown a significant inhibitory effect on the growth of cancer cells (Li et al. 2020b). Based on these studies, this article proposes a new type of MNs patch that can embed the LED light source within the MNs and achieve wireless power supply, aiming to improve the inconveniences in the treatment process and enhance therapeutic efficacy.

This article adopts a process that is simple to prepare, with a short preparation cycle, using UV curing method to prepare a polymer MNs patch integrated with an LED light source (LED-HEMA/MN, LH-MN). Hydroxyethyl methacrylate (Hydroxyethyl methacrylate, HEMA) is used as the base material to prepare LH-MN, focusing on its UV curing preparation process, and exploring the morphology, size, mechanical properties, ex vivo skin penetration performance, operating temperature, and performance

optimization of LH-MN. A new type of active integrated polymer MNs proposed in this paper can not only serve as a medium for the transmission of drugs or biological samples but also has the ability to transmit the LED light source from the skin surface to the deep skin, thereby achieving a synergistic effect of LT and drug treatment, while also supporting the separate delivery of drugs or light alone.

2 Experimental

2.1 Materials

Methyl methacrylate hydroxyethyl (CAS: 868-77-9) and photoinitiator 1173 (Chengdu Sichuan Four Cheng Photoelectric Material Co., Ltd.); Rose Bengal B (China National Medicine Group Chemical Reagent Co., Ltd.); Hydroxyethyl acrylate (CAS: 818-61-1, Shanghai Aladdin Biochemical Technology Co., Ltd.); Ex vivo pig skin (Beijing Weitong Lihua Experimental Animal Co., Ltd.); LED light source (Size: 3 mm × 3.2 mm × 2.8 mm, Color: Red) and wireless transmission coil (ADA Wireless Power Supply Light Bead Toy Company); Polydimethylsiloxane (CAS: 9006-65-9, components: PDMS, curing agent, Dow Corning Corporation (USA)); All solvents used in this paper are deionized water.

2.2 Equipment

Degassing stirrer (ZYMC-200V model, Shenzhen Zhongyi Technology Co., Ltd.); Electronic balance (AK20002 model, Chengdu Beisai Instrument and Equipment Research Institute); Optical microscope (SN-0745 model, Shenzhen Sannuo Xunu Technology Co., Ltd.); Scanning electron microscope (S-4700 model, Hitachi (China) Co., Ltd.); Roller to flat UV press machine (ERP-210 model, Wavelength: 365 nm, Engineering System Co., Ltd.); Electronic universal testing machine (EUT5000 model, Shenzhen Sansi Testing Technology Co., Ltd.); Ultrasonic cleaner (BXXW-30AL model, Beijing Boxiang Xingwang Co., Ltd.); LCD thermal energy accumulation recorder (NHR-7100/7100R model, Runhong Instrument Co., Ltd.); Compression force tester (HLD model, Yueqing Aidebao Instrument Co., Ltd.); Universal tensile and compression testing machine (manual 8501 model, Shenzhen Ailigu Instrument Co., Ltd.); Brass MNs male model (Custom-designed Specifications, Henan Weina BenTeng Biotechnology Co., Ltd.).

3 The preparation method for the MNs PDMS model

Mix PDMS and curing agent in a weight ratio of 10:1, place the mixture in a vacuum defoaming mixer, pour the solution into a culture dish that has previously placed a brass MNs positive mold with needle tips facing up, and place it in an electric heating constant temperature drying oven at about 40 °C for 5–6 h. After drying and molding, scrape off the excess PDMS with a blade and peel off the brass MNs male model to obtain the PDMS model, as shown in Fig. 1 for the preparation process diagram.

4 Active integrated fabrication method of polymer MNs

In order to better fix the encapsulated LED light source and ensure that the MNs has sufficient mechanical properties to puncture biological tissues for light transmission, select biocompatible and fast-curing photopolymerizable material HEMA and photoinitiator 1173 as the base materials (Xiao et al. 2023; Elouali et al. 2009). HEMA is an organic substance, a colorless, transparent, easily flowing liquid, widely used in the synthesis of medical polymer materials, thermosetting coatings, and adhesives, etc. (Baidu Baike 2-Hydroxyethyl methacrylate; Tauscher et al. 2017; Huang et al. 2020; Cochinski et al. 2024).

The prepared UV curable material is poured onto the surface of the MNs PDMS mold, and vacuum degassing treatment for about 1 min is carried out in a degassing stirrer to fully fill the cavity. Then, the LED light source is placed at the base of the MNs, use roller to flat UV press machine for UV curing treatment, causing the MNs to fully cure and encapsulate the LED light source in the base. Finally, the MNs array is demolded to obtain the MNs array integrated with the LED light source (LED-HEMA/MN, LH-MN), as shown in Fig. 2 for the preparation process diagram.

To prevent the MNs array from having residual monomers that are not fully polymerized, which could affect the biocompatibility of the MNs, the formed MNs needs to be ultrasonically cleaned. After cleaning, the MNs patch is sterilized under UV light exposure, and finally, a drug-

loaded hydrogel (such as chitosan, polyvinylpyrrolidone, etc.) is applied to the surface of the MNs. After drying and forming, a MNs with good biocompatibility is obtained.

5 Influence factors of polymer MNs fabrication

5.1 Influence of UV irradiation duration on the quality of MNs formation

During the process of preparing MNs using UV curing method, the duration of irradiation can affect the molding effect and the height of the MNs. To ensure complete curing of the photopolymerizable material to improve the molding rate of the MNs, the prepared material is poured onto the surface of the Polydimethylsiloxane (PDMS) mold, followed by about 1 min of vacuum degassing treatment to fully fill the mold cavity. Subsequently, the UV irradiation duration is set to 5, 10, 20, 30, 40, 50, 60, 80, 100, 120, and 180 s, respectively. Finally, the cured MNs are demolded to obtain the MNs array. The optimal UV irradiation duration is determined by two criteria: the molding rate and the height of the MNs.

The effect of UV irradiation duration on the molding rate and height of the MNs is shown in Fig. 3. The experimental results indicate that within the initial 10 s, the molding rate and height of the MNs increase rapidly. As the irradiation duration increases, the rate of increase in the molding rate and height of the MNs slows down. When the irradiation duration is around 60 s, the needle tip has essentially been fully cured. Although increasing the irradiation duration can further enhance the molding rate and height of the MNs, the additional increase is relatively small, and prolonged exposure may lead to yellowing and brittleness of the MNs. Therefore, the optimal UV irradiation duration during the preparation process should be controlled at 60 s.

5.2 Influence of photoinitiator content on the quality of MNs formation

To avoid interference from the UV irradiation duration when investigating the influence of photoinitiator content

Fig. 1 Preparation process diagram of PDMS model

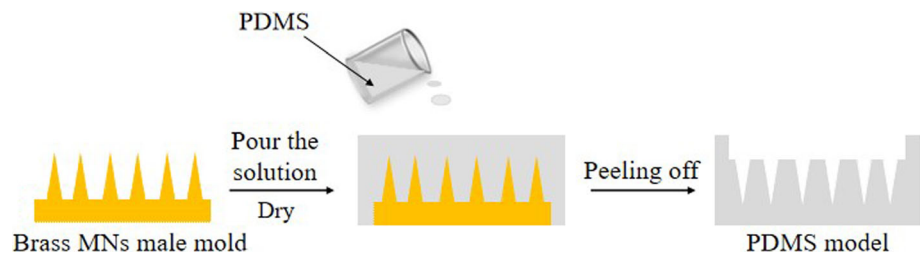


Fig. 2 Preparation process diagram of LH-MN

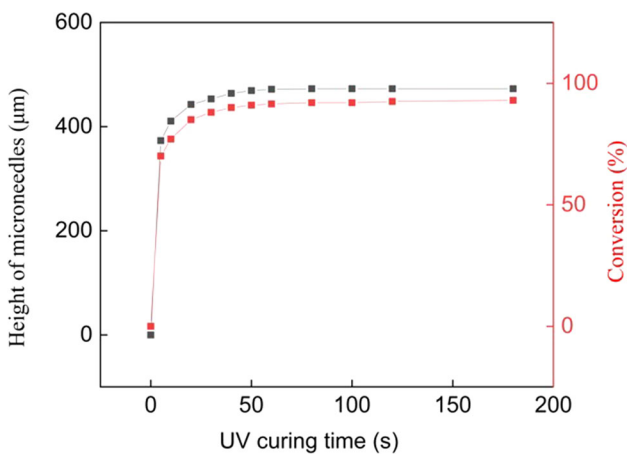
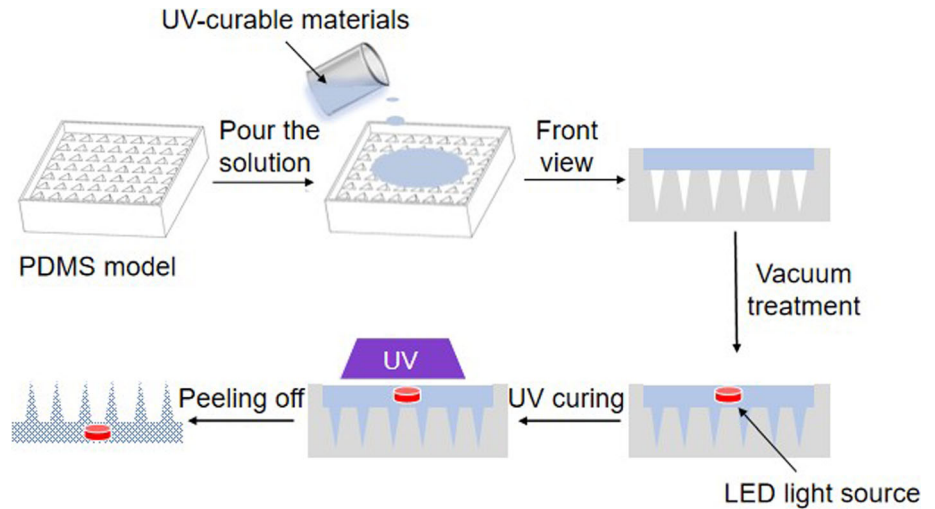


Fig. 3 Effect of lighting duration on the forming rate and height of MNs

on the quality of MNs formation, the irradiation duration is uniformly set to 1 min. Subsequently, photopolymerizable materials with photoinitiator concentrations of 0.5%, 1%, 2%, 3%, 4%, and 5% are prepared. The prepared material is poured onto the surface of the MNs PDMS mold and subjected to about 1 min of vacuum degassing treatment to fully fill the mold cavity. Afterward, the MNs are cured with 1 min of UV irradiation. Finally, the cured MNs are demolded to obtain the MNs array. The optimal photoinitiator concentration is determined by the molding rate of the MNs.

The effect of photoinitiator content on the molding rate and height of the MNs is shown in Fig. 4. The experimental results show that when the photoinitiator concentration is less than 3%, the molding rate of the MNs is poor; when the photoinitiator concentration is 3%, both the polymerization rate and the molding rate are optimal, with the molding rate of the MNs reaching over 92%; when the photoinitiator concentration is greater than 3%, it can filter

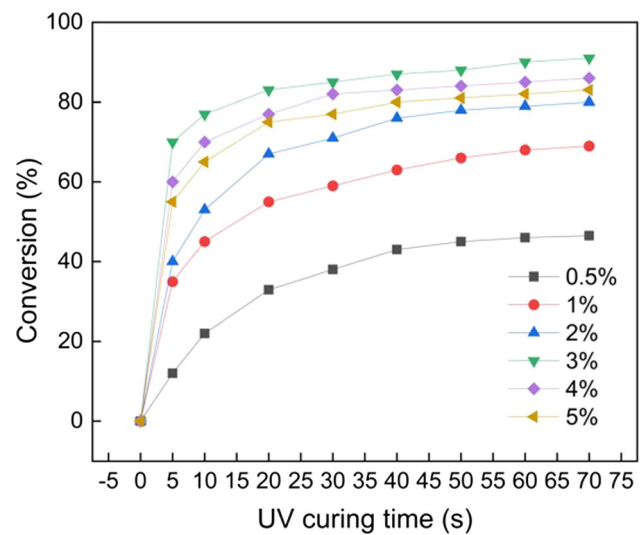


Fig. 4 Influence of photoinitiator concentration on the molding rate of MNs

out some of the light due to its own filtering effect, reducing the UV penetration ability and resulting in a lower molding rate. In addition, as the concentration of the photoinitiator increases, the adhesion of the MNs patch also increases, making it difficult to demold the needle body and thus reducing the molding rate. Therefore, the optimal photoinitiator concentration during the preparation process is 3%.

5.3 Influence of ultrasonic cleaning time on MNs cytotoxicity

To explore the influence of ultrasonic cleaning time on the cytotoxicity of the MNs array, the formed MNs are ultrasonically cleaned for 5, 10, 15, and 20 min. After cleaning, the MNs patches are sterilized under UV light exposure. L-929 cells are cultured in a CO₂ incubator (5% CO₂,

37 °C) for 24 h, centrifuged for 3 min to prepare a cell suspension, and the cell density is diluted to 5000 $\mu\text{g}/\text{mL}$. Then, the experimental group, physiological saline control group, and blank group cell suspensions are inoculated onto a 96-well plate, with 100 μL of cell suspension inoculated into each well and continued to culture for 24 h. Subsequently, 15 μL of the sample extract is added to each well for culture. After the cell culture is completed, the cells are placed under a microscope to observe their morphology and to measure their viability.

The cytotoxicity assessment of the LH-MN array treated with different ultrasonic cleaning times is shown in Fig. 5. Experimental results show that the cell survival rate of the LH-MN array ultrasonically cleaned for 5 min is relatively low, only about 70%, indicating that there may be residual monomers on the surface of the LH-MN array that have not fully polymerized, thus exerting a certain level of toxicity to the cells. As the cleaning time increases, cell activity increases, and after about 15 min of ultrasonic cleaning, the cell survival rate can reach over 85%. It can be concluded that proper ultrasonic cleaning can effectively remove residual monomers, and the optimal ultrasonic cleaning time in the preparation process is 15 min.

6 Polymer MNs performance optimization

Light-curing acrylic coatings/photo-sensitive coatings HEA, after curing, exhibit high wear resistance, adhesion, flexibility, and bio-safety, making it an excellent comprehensive performance radiation-curing material. The use of a small amount of HEA can significantly enhance the performance of the products (Yu et al. 2022; Ma et al. 2024; Zhang et al. 2023). To improve the adhesion of the MNs patch and enable it to be applied to different shapes of

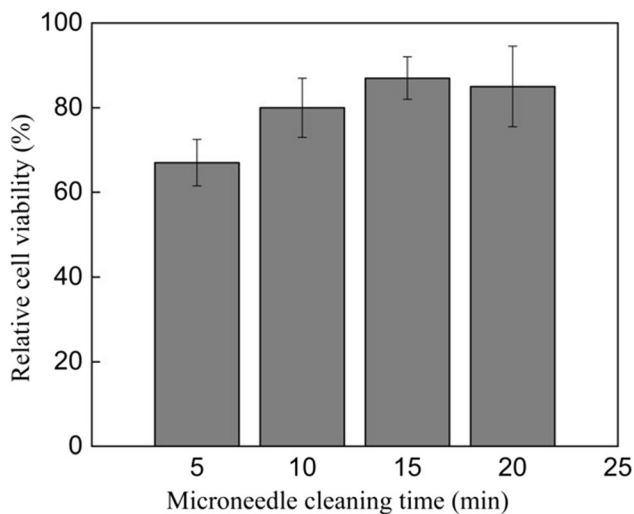


Fig. 5 Cell toxicity test results graph

target lesions, this paper uses HEA to modify HEMA, giving it both flexibility and strength, thereby enhancing the practicality of the MNs patch.

Firstly, HEMA and HEA are mixed in the proportions of 9:1, 8:2, 7:3, 6:4, and 5:5 (w/w), and finally, a photoinitiator is added to obtain a HEMA/HEA solution containing 3% photoinitiator 1173. The MNs preparation process is carried out as shown in Fig. 1, where the HEMA/HEA mixed solution containing 3% photoinitiator 1173 is poured onto the PDMS mold surface, vacuum degassed for about 2 min in a degassing stirrer to fully fill the mold cavity. Then, the LED light source is placed at the base of the MNs, and UV curing is performed using a roller to flat UV press machine for 1 min, causing the MNs to fully cure and encapsulate the LED light source in the base. Finally, the MNs array is demolded to obtain the flexible MNs array integrated with the LED light source (LED-HEMA/HEA-MN, LHH-MN). During the preparation process, it is ensured that the LHH-MN array of each proportion has a uniform composition and structure.

7 Testing and characterization

7.1 Testing and characterization of LH-MN

7.1.1 Morphology and size characterization

To characterize the size and molding effect of the LH-MN array, the surface smoothness and key size parameters of the MNs are first observed using an optical microscope. Under the optical microscope, the micro details of the MNs surface can be observed, including surface defects or smoothness. Subsequently, a scanning electron microscope (SEM) is used for further observation. Before SEM observation, the MNs are cut into a 2×2 array and fixed on the sample stage with conductive tape to ensure stability in a high vacuum environment. After gold sputtering treatment, they are placed in the SEM for observation of morphology and size.

7.1.2 Mechanical property testing

To test whether the LH-MN array has sufficient mechanical properties to penetrate skin tissue, a compression force tester is used to test the mechanical properties of the MNs. Before testing, the MN array is cut into a 2×2 array and fixed on the sample stage with double-sided tape. The bending speed is set to 0.5 mm/min, and the force–displacement change of the MNs is recorded.

7.1.3 Puncture performance testing

To explore the transdermal performance of the LH-MN array, pig skin is used to simulate the MNs's puncture to the skin. A piece of thawed pig skin is cut into a size of 3 cm × 3 cm with a surgical knife, disinfected with 75% alcohol, and then placed on filter paper to absorb excess moisture. During the experiment, the electronic universal testing machine is set to a pressure of 10 N, and the 8 × 8 MNs array is pressed onto the ex vivo pig skin. After 3 min, the skin surface is stained with Rose Bengal B solution, and the puncture situation is observed under an optical microscope.

7.1.4 LED light source temperature test

To avoid thermal damage to the tissue during the treatment process, the working temperature of the LED light source is monitored. The LED light source is placed in an electromagnetic induction coil to stably light up, and then the working temperature of the LED light source is measured using an LCD thermal energy accumulation recorder. Temperatures are recorded at 0, 12, 24, 48, 72, and 96 h.

7.2 Testing and characterization of LHH-MN

7.2.1 Appearance morphology characterization

To investigate the effect of adding HEA to HEMA on the flexibility of the MNs patch, a series of MNs patches with different flexibilities are prepared by adjusting the ratio of the two monomers. By applying controllable pressure to the LHH-MN array with fingers, it undergoes bending deformation. This experiment simulates the curvature changes and mechanical challenges that the MNs patch may encounter in actual use. Through this manual squeezing method, the deformation behavior of the MNs patch under the action of external force can be intuitively observed, including bending angle, shape recovery ability, and whether breakage occurs or not.

7.2.2 Flexibility test

To explore the flexibility of LHH-MN (assuming LHH-MN refers to a specific type of MNs), a hand-cranked universal tensile and compressive testing machine is used for the test. This type of testing machine provides a convenient and cost-effective method to evaluate the response of MNs patches when subjected to mechanical stress. Before conducting the test, the MNs patch to be tested is securely mounted in the clamps of the testing machine, ensuring that its position is fixed during the test to prevent any slipping or displacement. After confirming that there is no

interference from external forces, the rotating handle is turned at a uniform speed, and the test is stopped when the MNs patch breaks or reaches its bending limit. The force applied to the MNs and the corresponding displacement changes are recorded for analysis of its flexibility.

7.2.3 Mechanical performance test

To test whether the LHH-MN array has sufficient mechanical properties to penetrate skin tissue, a compression force testing machine is used to conduct the mechanical performance test of the MNs. Before the test, the MNs array is cut into a 2 × 2 array, and the MNs patch is fixed onto the specimen stage using double-sided adhesive tape. The bending speed is set to 0.5 mm/min, and the relationship between the force applied to the MNs and the displacement is recorded. The mechanical properties of MNs with different proportions of HEMA/HEA (assuming HEMA and HEA refer to specific materials or components in the MNs formulation) are compared.

8 Results and discussion

8.1 Results and discussion of LH-MN

8.1.1 Morphology and size

The LH-MN array's size and molding effect were characterized using an optical microscope and a scanning electron microscope (SEM), as shown in Fig. 6a–f. The needle body of the LH-MN array is triangular pyramidal in shape, with a base edge length of $(400 \pm 3) \mu\text{m}$, a height of $(480 \pm 10) \mu\text{m}$, a tip diameter of $(10 \pm 5) \mu\text{m}$, an apex angle of about $(41 \pm 2)^\circ$, and a molding rate of about 97%. The MNs are uniformly long, well-formed, and show no significant breakage.

8.1.2 Mechanical properties

The mechanical properties of the LH-MN array were tested using a compression force tester, and the force–displacement change curve during compression was obtained, as shown in Fig. 7a, b. During compression, the deformation of the MNs increases continuously with increasing pressure, and there is no obvious abrupt point in the graph, indicating that the MNs did not experience significant breakage throughout the compression process. It takes about 4.5 N of force to deform the MNs by 200 μm . Previous studies have indicated that the minimum pressure required for a single MN to penetrate the skin is 10 mN (Cole et al. 2016; Sun et al. 2017; Li and Zhang 2013; Moussi et al. 2019). Therefore, for a 2 × 2 array of MNs to

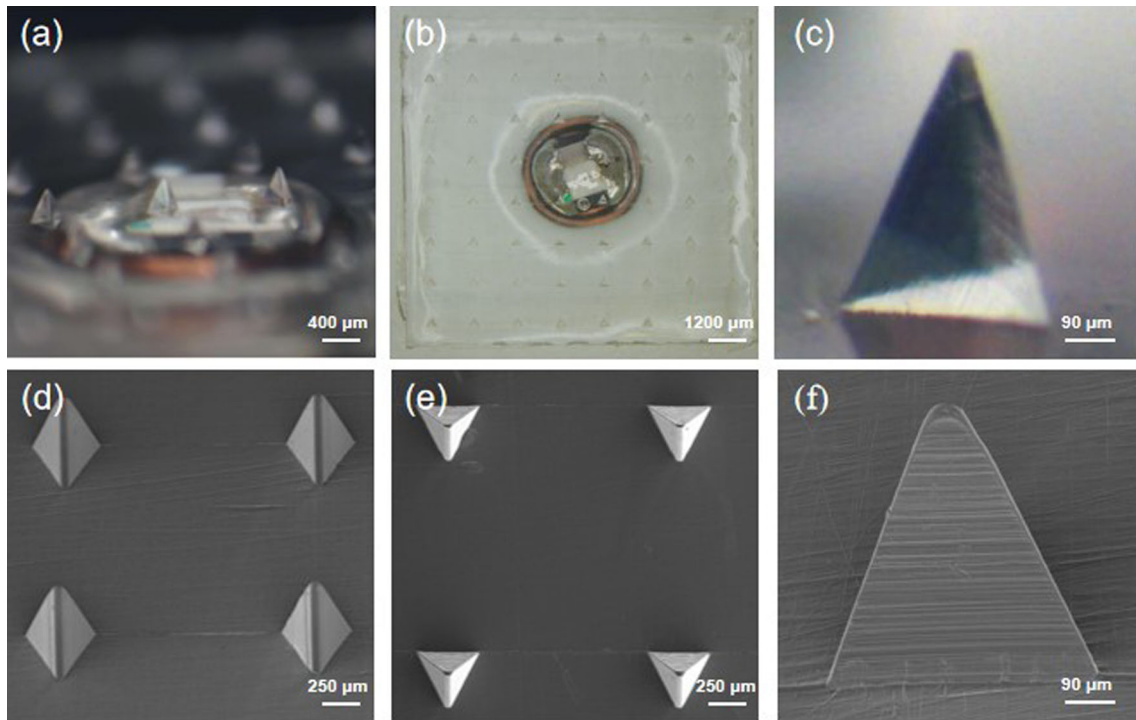
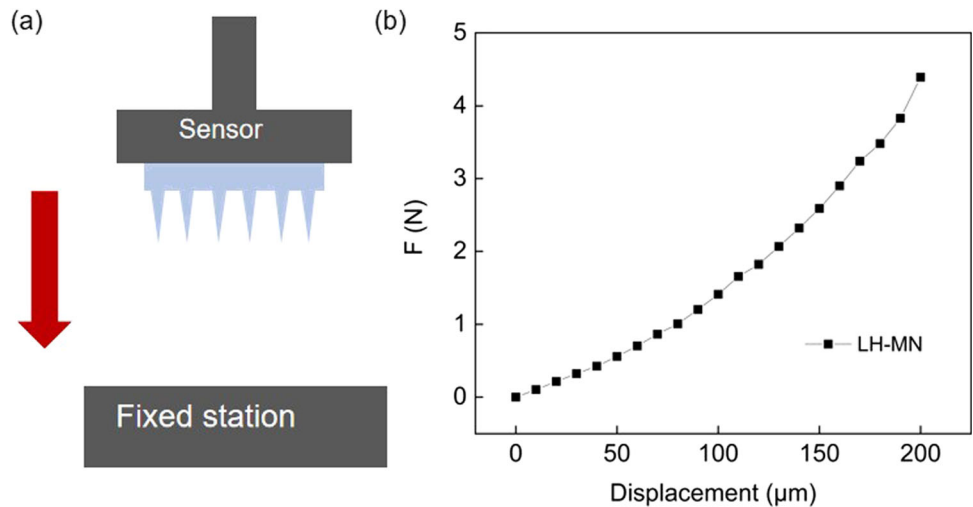


Fig. 6 Morphological Dimensions of LH-MN; **a–c** represent the three views of the MNs array optical microscope, respectively; **d–f** represent the three views of the MNs array scanning electron microscope, respectively

Fig. 7 Mechanical Properties of LH-MN; **a** Schematic diagram of LH-MN mechanical performance testing; **b** LH-MN force and displacement variation curve graph



penetrate the skin, the minimum pressure required is 40 mN. Experimental results show that the mechanical strength of the LH-MNs meets the experimental requirements and far exceeds what is needed, demonstrating their excellent reliability and safety.

8.1.3 Puncture performance

High-resolution microscopy was used to capture the overall effect after the MNs were inserted into the skin, as shown in Fig. 8a. It can be clearly seen that the MNs have

successfully penetrated the skin, leaving a row of neat microchannels. The formation of these microchannels is direct evidence of the successful penetration of the MNs patch through the skin surface and is also a key channel for light transmission to the internal skin tissue. The overall effect after staining with Rose Bengal B solution is shown in Fig. 8b. The dark areas in the figure clearly indicate the location of the microchannels, a step that not only enhances the visibility of the microchannels but also facilitates subsequent analysis. To observe the structure of the

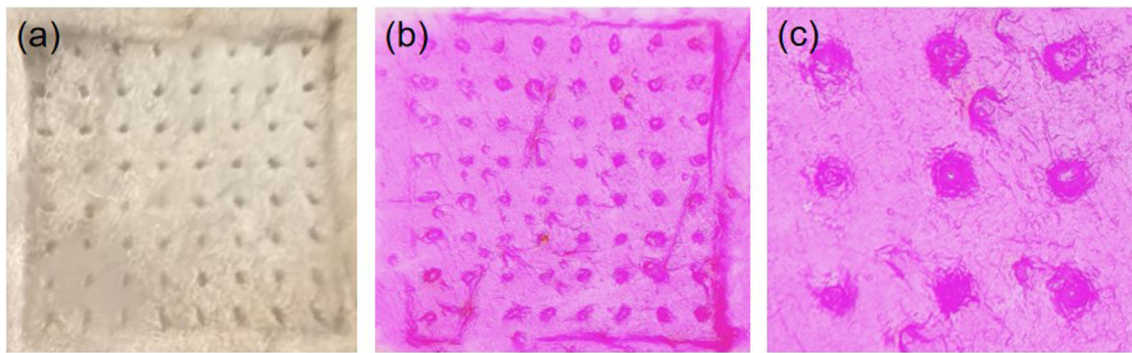


Fig. 8 In vitro puncture performance of MNs; **a** Overall effect after MNs insertion into pig skin; **b** Staining diagram after microneedling into the skin; **c** Enlarged view of the local area after microneedling into the skin

microchannels more clearly, some areas were enlarged, as shown in Fig. 7c.

8.1.4 LED light source operating temperature

To enable the LH-MN array to be implanted in subcutaneous tissue or even deeper tissues or organs, a wireless power supply system was constructed. The LED light source in the electromagnetic induction coil can be stably lit at various positions, and it remains effective within about 20 cm above and below, providing a stable light source. The LED light source of the LH-MN array is wirelessly powered and lit for an extended period, as shown in Fig. 9a, b. An LCD thermal energy accumulation recorder was used to measure the working temperature of the LED light source, and the temperature change curve was obtained, as shown in Fig. 10a, b. The experimental results show that after 12 h of illumination, the temperature of the LED light source rose from 21 to 22 °C, and after 24 h, it rose to 24 °C, and remained constant thereafter. It can be concluded that the LED light source has a limited temperature increase during long-term operation, is relatively safe, and does not pose a risk of thermal injury to tissue.

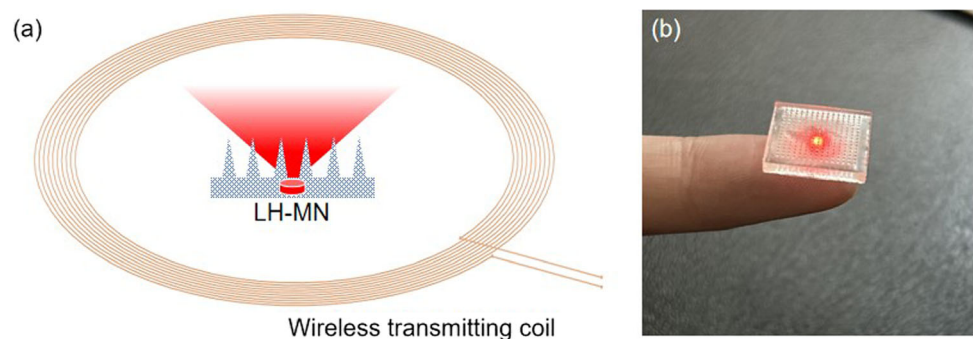
8.2 Results and discussion of LHH-MN

8.2.1 Appearance morphology

When HEMA and HEA are mixed in different proportions, the resulting MNs exhibit different degrees of flexibility, as shown in Fig. 11a–f. As the proportion of HEA gradually increases, the flexibility of the MNs patch also increases. This is due to the differences in the molecular structures of HEMA and HEA, which affect their interaction when mixed, thereby influencing the flexibility of the final material. The HEMA molecule contains a methyl group, which makes the molecular chains more closely arranged in space, increasing the rigidity and hardness of the material. The HEA molecule does not contain a methyl group, and the molecular chains are more loosely arranged, giving the material better flexibility. When HEMA and HEA are mixed in higher proportions, the rigidity and hardness of HEMA dominate, resulting in a relatively stiff material. Conversely, because the molecular chains of HEA are more easily movable and bendable, when the proportion of HEA is higher, the material's flexibility is better.

Therefore, by adjusting the ratio of HEMA to HEA, the flexibility of the final material can be controlled. In applications requiring higher flexibility, the proportion of HEA can be increased. In applications requiring higher

Fig. 9 Wireless power supply system; **a** Schematic diagram of LED light source for wireless power supply; **b** MNs patch diagram when LED light source is on



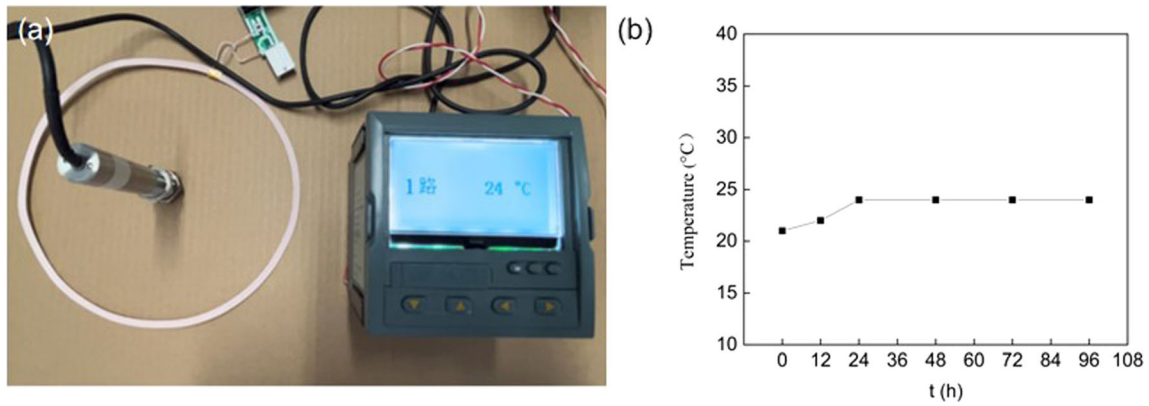
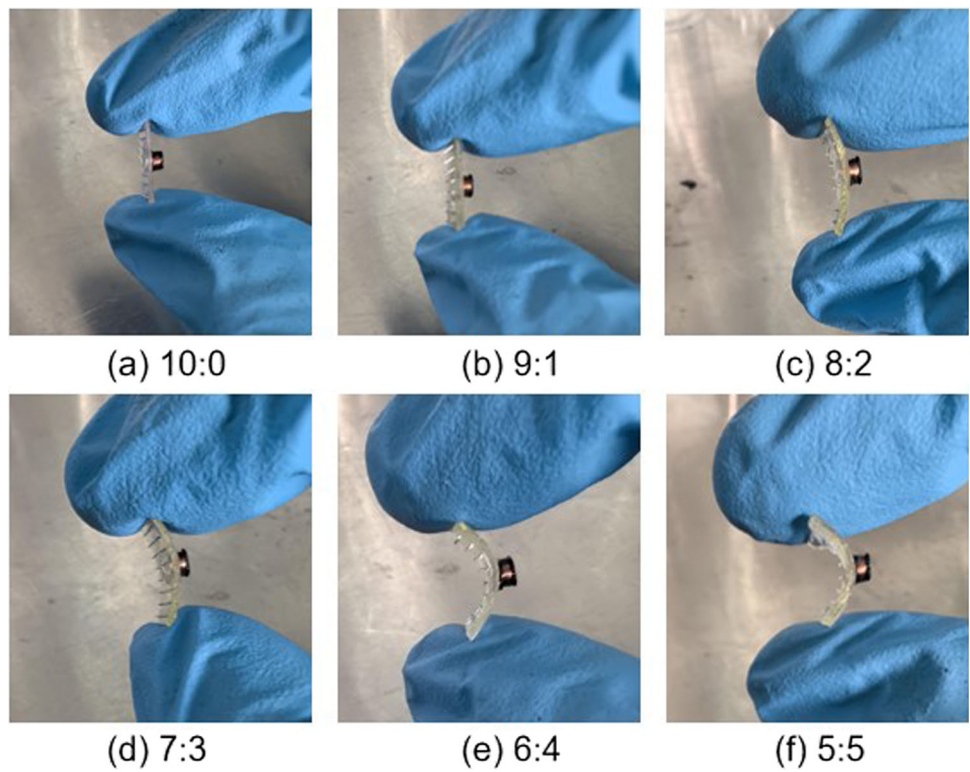


Fig. 10 Working temperature of LED emitting devices in LH-MN; **a** LED light-emitting device temperature testing system schematic; **b** LED light-emitting device temperature change curve

Fig. 11 a–f Flexible appearance characterization of LHH-MN under different proportions of HEMA/HEA



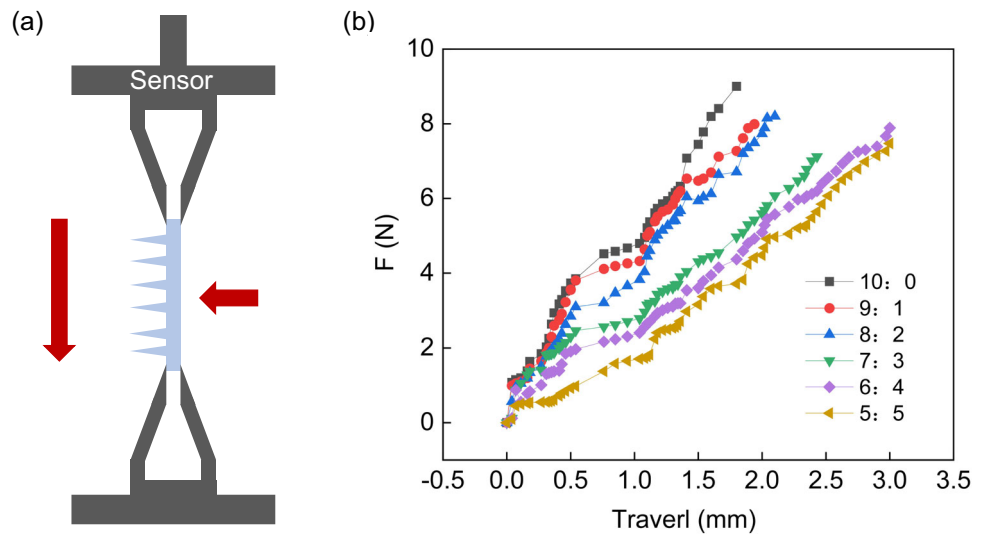
rigidity, the proportion of HEMA can be increased. This method of adjustment provides flexibility in the design and optimization of MNs to meet their needs in different application scenarios.

8.2.2 Flexibility analysis

The modified MNs patch was tested for flexibility using a tensile and compression testing machine, and the force–displacement change curve of the LHH-MN array during compression was obtained, as shown in Fig. 12a, b. Before the displacement is about 0.6 mm, the material undergoes

elastic deformation, and the force and displacement basically increase linearly. When the displacement is in the range of 0.6–1.1 mm, the material undergoes yield deformation. It can be seen that the unmodified MNs patch has poor flexibility, requiring about 9 N of force to bend the LHH-MN array by 1.7 mm, and brittle fracture occurs. As the proportion of HEA increases, the flexibility of the MNs is improved. When the HEMA to HEA ratio is 9:1, 8:2, 7:3, 6:4, and 5:5, it only requires about 7, 6.2, 4.5, 4, and 3.8 N of force, respectively, to bend the LHH-MN array by 1.7 mm, and the LHH-MN arrays with ratios of 6:4 and 5:5 do not break even when bent by 3 mm, indicating that

Fig. 12 Flexibility of LHH-MN; **a** Schematic diagram of the flexibility test for LHH-MN; **b** Force–displacement curve of LHH-MN



HEA can effectively improve the flexibility of HEMA to meet the needs of different shapes and positions of the lesion, significantly enhancing the practicality of the MNs.

8.2.3 Mechanical properties

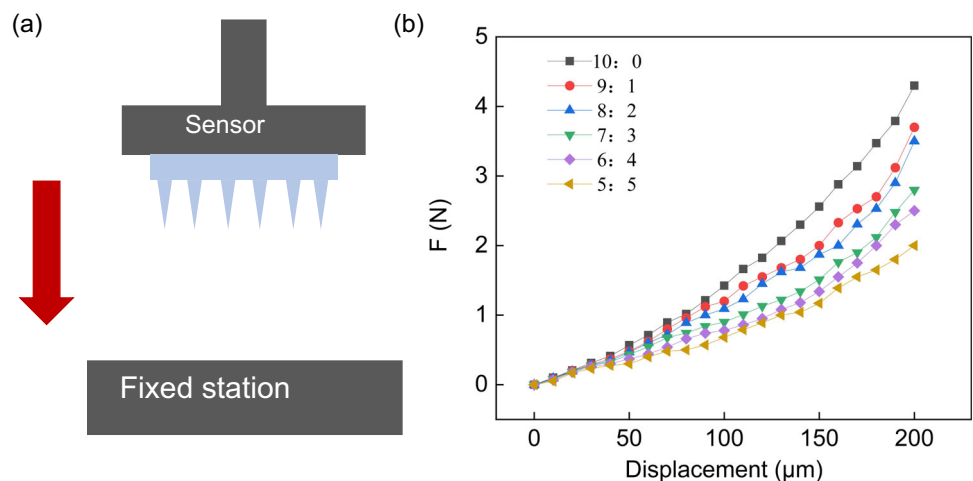
Mechanical property testing was conducted using a compression force testing machine, and the relationship between force and displacement during the compression process for LHH-MN arrays with different HEMA/HEA ratios was obtained, as shown in Fig. 13a, b. During compression, the deformation of the MNs increased continuously with increasing pressure, and no obvious abrupt points were observed in the graph, indicating that the MNs did not undergo significant breakage throughout the compression process. Furthermore, as the proportion of HEA (hydroxyethyl acrylate) continuously increased, the mechanical properties of the MNs decreased. When the ratio of HEMA (hydroxyethyl methacrylate) to HEA was

5:5, the force required to deform the MNs by 200 μm was approximately 1.9 N. Therefore, the modified LHH-MN possess a certain degree of mechanical strength that meets the experimental requirements.

9 Conclusion

This paper studies the polymer MNs integrated with an LED light source, proposing a new process for fabricating solid MNs arrays with high molding rate and short cycle using UV curing method. The morphology and size were characterized, and the mechanical properties, ex vivo skin penetration performance, and temperature of the light-emitting device were tested. On this basis, HEMA was modified with HEA to prepare MNs patches with good flexibility and high strength, and their appearance, flexibility, and mechanical properties were tested. The specific conclusions are as follows:

Fig. 13 Mechanical properties of LHH-MN; **a** Schematic diagram of LHH-MN mechanical performance testing; **b** Force and displacement variation curves for mechanical performance testing of LHH-MN with different ratios



- (1) The LH-MN prepared using the UV curing method has a high molding rate and short preparation cycle. The base has no bubbles, good smoothness, and the light source can be embedded in the base. The optimal preparation process obtained from the experiment is: a photoinitiator concentration of 3%, UV light irradiation time of 1 min, and ultrasonic cleaning time of 15 min. The overall preparation cycle is only about 25 min, and the molding rate is above 97%.
- (2) The LH-MN has good mechanical properties, skin penetration performance, and high safety. Mechanical experiments show that the MNs does not break obviously under the maximum compression of 4.5 N, and the ex vivo skin penetration performance also proves that the LH-MN can successfully penetrate the skin to form microchannels. The temperature test of the light-emitting device indicates that the LH-MN has high safety and does not pose a risk of thermal injury to tissue.
- (3) The modification results of the HEMA/HEA mixed MNs show that the flexibility of the LHH-MN is also improved with the increase of the HEA ratio. When the HEMA to HEA ratio is 6:4 and 5:5, it only requires about 4 N of force to bend the MNs by 3 mm, and it will not break. At the same time, the mechanical property test also shows that the modified LHH-MN does not break obviously under the compression of about 1.9 N, possessing both high strength and flexibility. It can meet the needs of different shapes and positions of the lesion, significantly improving the practicality of the MNs.

This article introduces an innovative fabrication process for MNs that embeds an LED light source within the MNs, paving the way for combined light and drug therapy as well as precise light delivery through MNs. Compared to traditional external light sources, the MN patch with a built-in LED light source offers a more flexible and patient-friendly treatment method. This innovative design not only overcomes the problem of limited patient mobility but also provides the possibility of deep tissue treatment through concentrated and uniform light exposure, which is expected to significantly enhance therapeutic effects. Researchers can select the most suitable LED light source, including wavelength, intensity, and efficiency, according to specific application scenarios and treatment needs. Through the optimization of the MN fabrication process, a high molding rate and excellent mechanical properties have been achieved, ensuring that the MNs can effectively penetrate the skin while maintaining a high level of biosafety. In addition, by adjusting the material ratio of the MNs, we have customized MN patches with different flexibility to

adapt to the skin conditions and treatment needs of different patients.

The MN patch in this study shows great potential in the field of phototherapy, especially in treatment plans that require precise control of light exposure conditions. For instance, in cases where localized phototherapy is needed to promote tissue repair or suppress inflammation, the MN patch can provide more accurate light exposure. In the future, with the development of wireless power supply technology, this MN patch is also expected to be applied to a wider range of remote medical and home medical scenarios. Through further research and development, we can explore the impact of different wavelengths of LED light sources on the treatment of specific diseases, as well as how to combine MNs with other treatment methods (such as drug therapy, gene therapy, etc.) to achieve more comprehensive therapeutic effects. Overall, this study has not only achieved innovative results in the development of MNs but also opened up a broad vision and a variety of possibilities for future clinical applications and scientific research.

Acknowledgements This work was supported by the Innovation and Transformation Fund of the Third Hospital of Peking University (BYSYZHKC2023112).

Author contributions J.Z., Q.X.H., X.Q.H., J.X.Z. and L.Z. provided direction and guidance throughout the preparation of this manuscript. X.N.Z. collected and interpreted studies and was a major contributor to the writing and editing of the manuscript. J.Z. and J.X.Z. reviewed and made significant revisions to the manuscript. All authors read and approved the final manuscript.

Data availability No datasets were generated or analysed during the current study.

Declarations

Conflict of interest The authors declare no competing interests.

References

- Baidu Baike 2-Hydroxyethyl methacrylate. https://baike.baidu.com/item/%E7%94%B2%E5%9F%BA%E4%B8%99%E7%83%AF%E9%85%B8%E7%BE%9F%E4%B9%99%E9%85%AF/9642501?fr=ge_ala
- Cheong WF, Pahl SA, Welch AJ (1990) A review of the optical properties of biological tissues. *IEEE J Quantum Electron* 26:2166–2185. <https://doi.org/10.1109/3.64354>
- Cochinski GD et al (2024) Does the absence of HEMA in universal adhesive systems containing MDP affect the bonding properties to enamel and dentine? A one-year evaluation. *Int J Adhes Adhes* 132:103656. <https://doi.org/10.1016/j.ijadhadh.2024.103656>
- Cole G et al (2016) Dissolving microneedles for DNA vaccination: Improving functionality via polymer characterization and RALA complexation. *Hum Vaccin Immunother* 13:50–62. <https://doi.org/10.1080/21645515.2016.1248008>

- Courtois E et al (2021) Mechanisms of PhotoBioModulation (PBM) focused on oral mucositis prevention and treatment: a scoping review. *BMC Oral Health*. <https://doi.org/10.1186/s12903-021-01574-4>
- Dehghanpour HR et al (2023) Evaluation of photobiomodulation effect on cesarean-sectioned wound healing: a clinical study. *Lasers Med Sci*. <https://doi.org/10.1007/s10103-023-03774-6>
- Dompe C et al (2020) Photobiomodulation—underlying mechanism and clinical applications. *J Clin Med* 9:1724. <https://doi.org/10.3390/jcm9061724>
- Elouali FZ, Aïnad Tabet D, Maschke U (2009) Optical and electro-optical properties of poly(2-hydroxyethylmethacrylate)/5CB systems. *Mol Cryst Liq Cryst* 502:77–86. <https://doi.org/10.1080/15421400902815746>
- Glass GE (2020) Photobiomodulation: a review of the molecular evidence for low level light therapy. *J Plast Reconstr Aesthet Surg* 74:1050–1060. <https://doi.org/10.1016/j.bjps.2020.12.059>
- Glass GE (2021) Photobiomodulation: the clinical applications of low-level light therapy. *Aesthet Surg J*. <https://doi.org/10.1093/asj/sjab025>
- Huang M et al (2020) High-performance, UV-curable cross-linked films via grafting of hydroxyethyl methacrylate methylene malonate. *Ind Eng Chem Res* 59:4542–4548. <https://doi.org/10.1021/acs.iecr.9b06618>
- Li Y, Zhang PY (2013) Study on mechanical properties for modeling and simulation of microneedles for medical applications. *Appl Mech Mater* 454:86–89. <https://doi.org/10.4028/www.scientific.net/amm.454.86>
- Li Y et al (2020a) An implantable wireless powered light source. *Optoelectron Lett* 16:81–86. <https://doi.org/10.1007/s11801-020-9071-8>
- Li B et al (2020b) Nitric oxide release device for remote-controlled cancer therapy by wireless charging. *Adv Mater* 32:2000376. <https://doi.org/10.1002/adma.202000376>
- Li Y et al (2024) A versatile cryomicroneedle patch for traceable photodynamic therapy. *Adv Mater*. <https://doi.org/10.1002/adma.202400933>
- Lim D-J, Kim H-J (2022) Microneedles in action: microneedling and microneedles-assisted transdermal delivery. *Polymers* 14:1608. <https://doi.org/10.3390/polym14081608>
- Luo X, Yang L, Cui Y (2023) Microneedles: materials, fabrication, and biomedical applications. *Biomed Microdevices* 25:1. <https://doi.org/10.1007/s10544-023-00658-y>
- Ma J et al (2024) Effect of reactive diluent on properties of electron beam (EB) cured pressure sensitive adhesives. *Paint Coat Ind* 54(4):1–8. <https://doi.org/10.12020/j.issn.0253-4312.2023-246>
- Moussi K et al (2019) Biocompatible 3D printed microneedles for transdermal, intradermal, and percutaneous applications. *Adv Eng Mater* 22:1901358. <https://doi.org/10.1002/adem.201901358>
- Roets B (2023) Potential application of PBM use in hair follicle organoid culture for the treatment of androgenic alopecia. *Mater Today Bio* 23:100851. <https://doi.org/10.1016/j.mtbio.2023.100851>
- Sun J et al (2017) Numerical simulation and experimental study of filling process of micro prism by isothermal hot embossing in solid-like state. *Adv Polym Technol* 37:1581–1591. <https://doi.org/10.1002/adv.21815>
- Tauscher S et al (2017) Evaluation of alternative monomers to HEMA for dental applications. *Dent Mater* 33:857–865. <https://doi.org/10.1016/j.dental.2017.04.023>
- Wu X et al (2022) Localised light delivery on melanoma cells using optical microneedles. *Biomed Opt Express* 13:1045–1045. <https://doi.org/10.1364/boe.450456>
- Xiao T et al (2023) UV-cured polymer aided phase change thermal energy storage: preparation, mechanism and prospects. *J Energy Storage* 64:107066. <https://doi.org/10.1016/j.est.2023.107066>
- Xue Y et al (2024) Transdermal drug delivery system: current status and clinical application of microneedles. *ACS Mater Lett*. <https://doi.org/10.1021/acsmaterialslett.3c01317>
- Yamagishi K et al (2018) Tissue-adhesive wirelessly powered optoelectronic device for metronomic photodynamic cancer therapy. *Nat Biomed Eng* 3:27–36. <https://doi.org/10.1038/s41551-018-0261-7>
- Yin M et al (2023) Dissolving microneedle patch integrated with microspheres for long-acting hair regrowth therapy. *ACS Appl Mater Interfaces* 15:17532–17542. <https://doi.org/10.1021/acsaami.2c22814>
- Yu et al (2022) Study on migration behavior and cytotoxicity of photoinitiators in photocurable coatings. *Paint Coat Ind* 52(05):39–47. <https://doi.org/10.12020/j.issn.0253-4312.2022.5.39>
- Zhang L et al (2021) Fabrication, evaluation and applications of dissolving microneedles. *Int J Pharm* 604:120749. <https://doi.org/10.1016/j.ijpharm.2021.120749>
- Zhang XP et al (2022) An update on biomaterials as microneedle matrixes for biomedical applications. *J Mater Chem* 10:6059–6077. <https://doi.org/10.1039/d2tb00905f>
- Zhang Y et al (2023) Preparation and properties research of UV-curable polyurethane acylate peelable coatings. *Paint Coat Ind* 53(2):27–31. <https://doi.org/10.12020/j.issn.0253-4312.2022-278>
- Zheng et al (2024) Clinical effect analysis of domain hair microneedles combined with red light in the treatment of androgenic alopecia. *China J Mod Med* 34(8):53–58. <https://doi.org/10.3969/j.issn.1005-8982.2024.08.009>

Publisher's Note Springer Nature remains neutral with regard to jurisdictional claims in published maps and institutional affiliations.

Springer Nature or its licensor (e.g. a society or other partner) holds exclusive rights to this article under a publishing agreement with the author(s) or other rightsholder(s); author self-archiving of the accepted manuscript version of this article is solely governed by the terms of such publishing agreement and applicable law.